A transient dynamic study of the self-excited vibration of a railway wheelset-track system induced by saturated creep forces

W.J. Qian[1], G.X. Chen[1]*, H. Ouyang[2], M.H. Zhu[1], W.H. Zhang[1], Z.R. Zhou[1]

[1]*Tribology Research Institute, State Key Laboratory of Traction Power, Southwest Jiaotong University, Chengdu, 610031, China*

[2]*School of Engineering, University of Liverpool, Brownlow Street, Liverpool L69 3GH, UK*

*Corresponding author. E-mail address: chen_guangx@163.com

Abstract: Two dynamic models of a wheelset-track system on a tight curved track and on a straight track are established. Both the transient dynamic and complex eigenvalue analyses are performed to study the unstable transient dynamics and stability of the wheelset-track system. It is assumed that in the models creep forces between wheels and rails are saturated, that is, approximately equal to the normal forces multiplied by the dynamic coefficients of friction. The simulation results demonstrate that the saturated creep force can induce self-excited vibration of the wheelset-track system. The normal contact force between the wheel and rail fluctuates at the same frequency as the wheel and rail vibrate when the self-excited vibration occurs. And the fluctuation frequency of the normal contact force falls into the range of 60-500 Hz, which corresponds to the frequency range of rail corrugation. This phenomenon indicates that the self-excited vibration of the wheelset-track system may be a main cause of rail corrugation occurrence. Parameter sensitivity analysis shows that the stiffness and damping of the rail fastener have important influences on the oscillation amplitude of the normal contact force. Bringing the friction coefficient below a certain level and increasing the damping of the rail fastener can suppress rail corrugation.

Key words: Railway wheelset-track; Self-excited vibration; Rail corrugation; Saturated creep force; Transient dynamics.

1. Introduction

Rail corrugation is an elusive problem in railway industry. Its formation and development cause fierce vibrations of the structures of both railway vehicle and track. These fierce vibrations in turn cause reduction of the operational life of structural components and the comfort of the passengers. Nowadays, grinding is generally used to remove rail corrugation of all types of rails all over the world. However, the cost of

grinding is very high. Eliminating or suppressing corrugation is still the best solution. Rail corrugation has been observed and studied for over 100 years, and many efforts have been made to understand the formation mechanisms of various types of corrugation. According to the review of published papers on rail corrugations [1-4], the generation mechanisms of rail corrugation can be roughly grouped into two major schools of thought.

The first school of thought believes that in railway lines, the original rail head is discontinuous. When a wheel rolls over a rail, the uneven properties of the rail head can induce fluctuations of contact forces between the wheel and rail. These fluctuating contact forces cause different wear rates of rail surfaces to generate corrugation. Knothe and his group [5, 6] made a detailed investigation into the material wear situation at different positions in a sleeper bay in terms of receptance and the pinned–pinned mode. Muller [7] and Nielsen [8] used a nonlinear contact mechanics filter to explain the independence of wave length of the short pitch corrugation. Jin et al. [9] investigated the effect of track irregularities on initiation and evolution of rail corrugation. In their study the effect of periodical variation of sleeper support on rail corrugation on a curved track was analyzed by including a vertical track irregularity due to the periodically passing of sleepers. Xie and Iwnicki [10, 11] established a three-dimensional contact model and a time-domain wheel-track vertical interaction model to calculate wear over the railhead.

The second school of thought believes that rail corrugation is caused by the instability of wheel-rail systems. The researchers who accept this school of thought are fewer than those who accept the first school of thought. However, the impact of this school of thought continues to date. Clark et al. [12, 13] studied the effect of the stick-slip phenomenon on rail corrugation. Brockley [14] earlier investigated rail corrugation from the view point of friction-induced vibration and derived a formula expressing the relation between corrugation wear and friction-induced vibration. Ishida et al. [15] found that fluctuation of the lateral or vertical forces might lead to stick-slip between rail and wheel and wear took place to form corrugation. Wu and Thompson [16] studied rail corrugation from the view point of micro-slip. Chen et al. [17] studied the formation mechanism of rail corrugation from the viewpoint of saturated-creep-force-induced self-excited vibration of a wheelset-track system. In their study, a finite element model of a wheelset-track system was established and analyzed using the complex eigenvalue method. Kurzeck et al. [18, 19] established a friction coupling model of a vehicle-track

system with three degree of freedom. They studied the effect of friction induced vibration of a vehicle-track system on rail corrugation. A comparison between the numerical results and the measurement results was carried out in their publications. However, up to now, the generation mechanism of rail corrugation is still not fully understood.

In this paper, two elastic vibration models of a wheelset-track system are established. Transient dynamic and complex eigenvalue analyses are performed by using the ABAQUS software. The simulation results demonstrate that when creep forces between the wheelset and rail become saturated, that is, equal to the normal forces multiplied by the dynamic coefficient of friction, these saturated creep forces can induce self-excited vibration of the wheelset-track system. And the normal contact force between the wheel and rail fluctuates when self-excited vibration occurs. The fluctuating normal contact force can induced the wear-type rail corrugation. Furthermore, some forms of rail corrugation can be explained by using the simulation results of this paper, such as why short pitch corrugation generally occurs on low rail of a tight curved track and why a low friction coefficient can eliminate rail corrugation [20, 21].

2. Finite element modeling of a wheelset-track system

2.1 Model of wheel-rail contact

Field measurement data demonstrate that when a train travels on a tight curved track, the leading wheelsets of both the front and rear trucks have positive angles of attack and the trailing wheelsets have positive or negative angles of attack mainly depending on running speed as shown in Fig. 1a [22]. The directions of lateral creep forces are fixed when the wheelsets have positive angles of attack. Fig. 1b shows the contact points and directions of lateral creep forces between the wheel and rail when a train negotiates a tight curved track [22]. It can be found that the contact point between the outer wheel of the wheelset and high rail shift to the flange root for wheel and to the gauge corner for rail, whilst the contact point between the inner wheel and low rail is roughly kept in the vicinity of the center of rail top for rail. When a train negotiates a tight curved track, the lateral creep force between the leading wheelset and rail probably becomes saturated [22]. In this case, the lateral creep force equals the normal force multiplied by the dynamic friction coefficient. And the longitudinal creep force is much lower than the lateral creep force if the wheelset is unpowered. Fig. 2a shows the

wheelset positions when the vehicle travels on a straight track. In that case, the lateral displacement of wheelset is low. Therefore, the contact points between the wheel and rail are easily determined by contact geometry calculation as shown in Fig. 2b. When trains are accelerated by large longitudinal traction forces or are braked by brake forces, the creep forces between the wheel and rail become generally saturated and hence are also approximately equal to normal forces multiplied by the dynamic coefficient of friction.

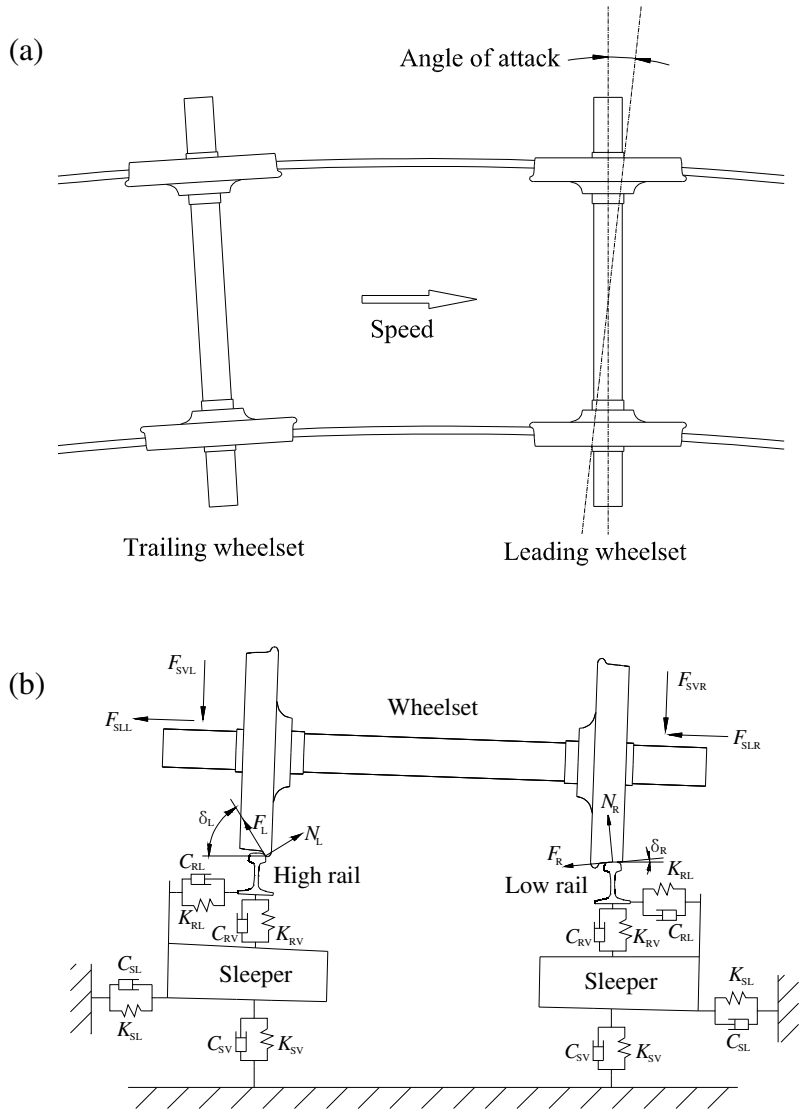

Fig. 1 Model of wheel-rail contact on a tight curved track: (a) wheelset positions; (b) positions of contact points and directions of lateral creep forces.

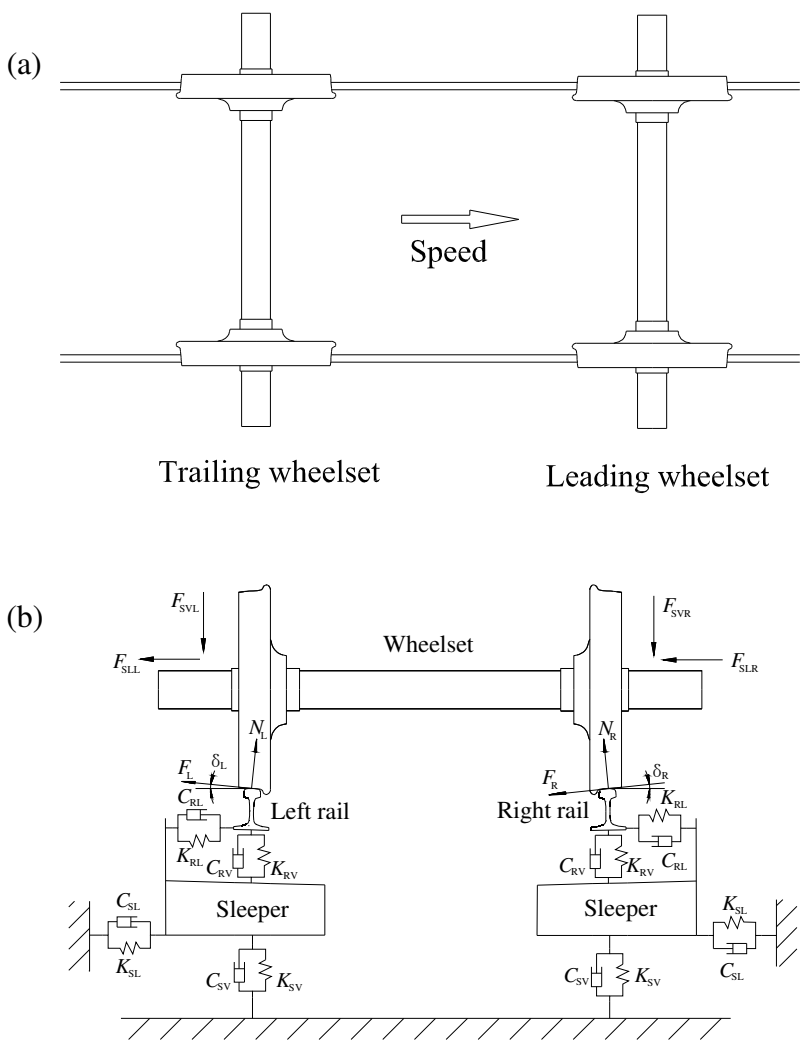

Fig. 2 Model of wheel-rail contact on a straight track: (a) wheelset positions; (b) positions of contact points and directions of lateral creep forces.

In the present paper, contact geometry parameters of the wheelset on a curved track are determined by curve negotiation calculation using the NUCARS package [23]. The parameters of wheelset and rail are presented as follows. The present model considers a wheelset and a curved track with 1435+2mm gauge and 300m radius. The rail cant is α_t = 1/40, and the sleeper pitch l_s = 600 mm. It is assumed that the speed of the vehicle running on a curved track is v = 70km/h. According to the NUCARS simulation results, when the vehicle negotiates the curved track at a speed of 70km/h, the contact angles are δ_L = 36.41° and δ_R = 1.52°. The angle of attack of the leading wheelset is y_w = 0.30°. The suspension forces are F_{SVL} = 103,200N, F_{SVR} = 91,800N, F_{SLL} = 7640N, and F_{SLR} = 7640N. Stiffnesses of the rail fastener are set to K_{RV} = 7.8×10^7N/m and K_{RL} = 2.947×10^7N/m. Damping values of the rail fastener are set to

C_{RV} = 5.0×10^{4}Ns/m and C_{RL} = 5.2×10^{4}Ns/m. Combined support stiffness of the sleeper and roadbed are set to K_{SV} = 8.9×10^{7}N/m and K_{SL} = 5.0×10^{7}N/m. Combined damping values of the sleeper and roadbed are set to C_{SV} = 8.98×10^{4}Ns/m and C_{SL} = 4.0×10^{4}Ns/m. On a straight track, it is assumed that the contact angles are δ_L = 4.26° and δ_R = 4.26°, and suspension forces F_{SVL} = 100,000N, F_{SVR} = 100,000N, F_{SLL} = 0N, and F_{SLR} = 0N. The stiffnesses and damping values of the rail fastener on a straight track are the same as that on the curved track. Combined support stiffnesses of the sleeper and roadbed on a straight track are set to K_{SV} = 1.2×10^{8}N/m and K_{SL} = 6.0×10^{7}N/m. Combined damping values of the sleeper and roadbed are set to C_{SV} = 1.0×10^{5}Ns/m and C_{SL} = 1.0×10^{5}Ns/m.

2.2 Finite element model of a wheelset-track system

There are two distinct contact conditions for the low (right) and high (left) rails as shown in Fig. 1 and 2. Therefore, two different finite element models of the wheelset-track system were established as shown in Fig. 3. Fig. 3a shows the finite element model of the wheelset-track system. In the finite element models, the total length of the rail is L = 36m, and the end effects of the rail are ignored and hinged–hinged constraints are applied. The rail mass per length is 60kg/m. On the contact interfaces between the rails and sleepers, the coordinates of the rail nodes are the same as the sleeper nodes. The rail node and the sleeper node which have the same coordinate constitute a pair of nodes. These node pairs are connected by the lateral and vertical springs and the lateral and vertical dampers as shown in Fig. 3b. There is a pad at each rail-sleeper contact interface represented by a spring and a damper. In the initial state, the length of the spring is zero. The node pairs can be separated when the springs are stretched. It also can be approached when the springs are compressed. Therefore, the rail foot and sleepers can separate or approach when the vibration occurs. The stiffness and damping values of the rail fastener are evenly distributed on every node. The sleepers are supported by a group of lateral and vertical springs and a group of lateral and vertical dampers at the bottom of sleepers (Fig. 3b). The number of lateral or vertical springs in each group of springs is the same as the number of nodes on the sleeper bottoms. The contact details between the wheel and rail on a tight curved track and on a straight track are shown in Fig. 3c and d. A wheel with worn tread profile of a freight car of nominal diameter 840mm is analyzed. Density of the wheel and rail materials is ρ = 7800kg/m^3. Young's modulus of both is E = 2.1×10^{11}Pa. Poisson's ratio of both is γ = 0.3. The track

under this investigation is the double-block non-ballasted track. Density of the sleeper is ρ = 2800kg/m^3. Young's modulus of the sleeper is E = 1.9×10^{11}Pa. Poisson's ratio of the sleeper is γ = 0.3. The measurement points of the vibration acceleration are located on the contact surface of the rail.

2.3 Finite element equations of the transient dynamic analysis

When a vehicle negotiates a tight curved track or a wheelset undergoes a large traction force or brake force on a straight track, the creep force between the wheel and rail probably becomes saturated [22]. In the present work, the creep forces between the wheels and rails are always assumed to be saturated. In this case, the creep forces are similar to friction forces and approximately equal to the normal forces multiplied by the dynamic coefficient of friction. In this paper, the Abaqus/Standard finite element solver is applied to obtain the transient dynamic response of the wheelset-track system. The calculation process is introduced briefly as follows.

In the Abaqus/Standard analysis procedure, the friction forces are governed by Coulomb's friction law. The friction stresses can be expressed in the form [24, 25]:

$$\tau_i = k_s \gamma_i^{el} \tag{1}$$

where $k_s = \tau_{crit} / \gamma_{crit}$ is the current stiffness, $\tau_{crit} = \mu p$ is the critical stress, μ is the friction coefficient, p is the contact pressure, γ_{crit} is referred to as the allowable maximum elastic slip. It is set to 0.5% of the average length of all contact elements in the model, γ_i^{el} is defined as the reversible relative tangential motion from the point of zero frictional stress.

Since τ_{crit} may be dependent on contact pressure and slip rate at the contact point, k_s may change during the analysis. The behavior remains elastic as long as the equivalent stress (τ_{eq}) does not exceed the critical stress (τ_{crit}). In this case, the relative tangential motion γ_i^{el} can be written in the form:

$$\gamma_i^{el}(t + \Delta t) = \gamma_i^{el}(t) + \Delta\gamma_i \tag{2}$$

where Δt is the time increment, $\Delta\gamma_i$ is the slip increment in direction *i.*

Consistent linearization of Eq. (1) yields:

$$d\tau_i = k_s d\gamma_i + (\tau_i / \tau_{crit})(\mu + p\partial\mu / \partial p)dp \tag{3}$$

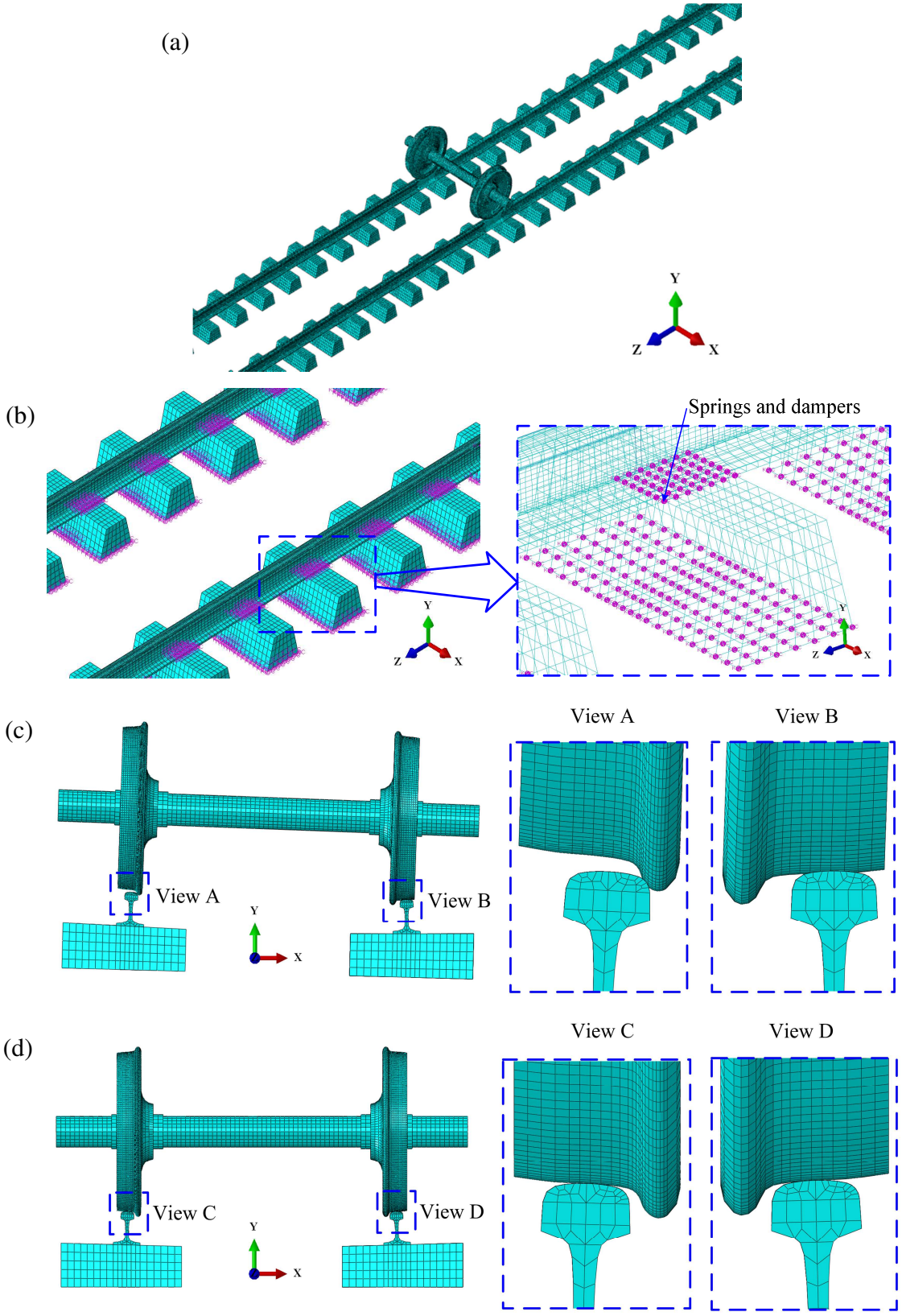

Fig. 3 Finite element model of the wheelset-track system: (a) an overview of the wheelset-track system model; (b) details of the contact interfaces between the rails and sleepers; (c) contact details between the wheel and rail on a tight curved track; (d) contact details between the wheel and rail on a straight track.

The contributions from the contact pressure are in Eq. (3) nonsymmetric. Since the slip rate is zero, derivatives with respect to the slip velocity are not needed.

If the equivalent frictional stress exceeds the critical stress, slip must be taken into consideration so that the condition $\tau_{eq} = \tau_{crit}$ is maintained in this situation. Let the starting situation be characterized by the elastic slip $\bar{\gamma}_i^{el}$. Let the elastic slip at the end of the increment be γ_i^{el} and the slip increment be $\Delta\gamma_i^{sl}$. Consistency requires that:

$$\Delta\gamma_i = \gamma_i^{el} - \bar{\gamma}_i^{el} + \Delta\gamma_i^{sl} \tag{4}$$

The frictional stress at the end of the increment follows from the elasticity relation, $\tau_i = k_s \gamma_i^{el} = (\tau_{crit} / \gamma_{crit})\gamma_i^{el}$. And the slip increment is related to the stress at the end of the increment with the backward difference approach.

$$\Delta\gamma_i^{sl} = (\tau_i / \tau_{crit})\Delta\gamma_{eq}^{sl} \tag{5}$$

With these equations and the critical stress equality $\tau_{eq} = \tau_{crit}$ it is possible to solve for γ_i^{el}, $\Delta\gamma_i^{sl}$, and τ_i. Elimination of γ_i^{el} and $\Delta\gamma_i^{sl}$ from the Eq. (4) yields,

$$\Delta\gamma_i = (\tau_i / \tau_{crit})\gamma_{crit} - \bar{\gamma}_i^{el} + (\tau_i / \tau_{crit})\Delta\gamma_{eq}^{sl}$$

$$\tau_i = \left(\left(\bar{\gamma}_i^{el} + \Delta\gamma_i\right) / \left(\gamma_{crit} + \Delta\gamma_{eq}^{sl}\right)\right)\tau_{crit} \tag{6}$$

It is convenient to define the elastic predictor strain, $\gamma_i^{pr} = \bar{\gamma}_i^{el} + \Delta\gamma_i$, which simplifies the expression for the frictional stress to

$$\tau_i = \left(\gamma_i^{pr} / \left(\gamma_{crit} + \Delta\gamma_{eq}^{sl}\right)\right)\tau_{crit} \tag{7}$$

Substitution in the critical stress equality yields

$$\Delta\gamma_{eq}^{sl} = \gamma_{eq}^{pr} - \gamma_{crit} \tag{8}$$

where $\gamma_{eq}^{pr} = \sqrt{\left(\gamma_1^{pr}\right)^2 + \left(\gamma_2^{pr}\right)^2}$.

Substitution in the expression for τ_i and introduction of the normalized slip direction $n_i = \gamma_i^{pr} / \gamma_{eq}^{pr}$ furnishes the final result:

$$\tau_i = n_i \tau_{crit} \tag{9}$$

Here τ_{crit} is a function of the slip rate, which is obtained from $\dot{\gamma}_{eq}^{sl} = \Delta\gamma_{eq}^{sl} / \Delta t$. For the iterative solution scheme this equation must be linearized. Some straightforward algebraic manipulation yields

$$d\tau_i = \left(d\gamma_i^{pr} / \gamma_{eq}^{pr}\right)\tau_{crit} - n_i n_j \left(\tau_{crit} / \gamma_{eq}^{pr}\right)d\gamma_j^{pr} + n_i d\tau_{crit}$$

$$= \left(\delta_{ij} - n_i n_j\right)\left(\tau_{crit} / \gamma_{eq}^{pr}\right) d\gamma_j^{pr} + n_i\left(\left(\partial \tau_{crit} / \partial p\right) dp + \left(\partial \tau_{crit} / \partial \dot{\gamma}_{eq}^{sl}\right) d\dot{\gamma}_{eq}^{sl}\right) \tag{10}$$

With the expression for the equivalent slip the final result is

$$d\tau_i = \left(\delta_{ij} - n_i n_j\right)\left(\tau_{crit} / \gamma_{eq}^{pr}\right) d\gamma_j + n_i\left(\mu + p\partial\mu / \partial p\right) dp + n_i n_j \left(p / \Delta t\right)\left(\partial\mu / \partial \dot{\gamma}_{eq}\right) d\gamma_j \tag{11}$$

In Eq. (11), the first term is generated by the friction forces acting in the direction perpendicular to the direction of slip. The second term yields the asymmetric contribution to the stiffness matrix. This term is essential to capture the phenomenon of the friction induced self-excited vibration. The third term exists if the friction coefficient depends on velocity. Both the first and third terms contribute to the damping matrix.

Friction is a typical nonlinear problem. A nonlinear dynamic analysis in Abaqus/Standard uses implicit time integration to calculate the transient dynamic response of a system [26, 27]. To discuss the dynamic procedure further, the inertia force in the overall equilibrium equation is examined. The body force at a point (f) can be written as an externally prescribed body force (F) and an inertia force:

$$f = F\text{-}\rho\ddot{u} \tag{12}$$

where ρ is the current density of the material at this point, and u is the displacement of the point. The body force term in the virtual work equation is

$$\int_V f \cdot \delta v dV = \int_V F \cdot \delta v dV - \int_V \rho\ddot{u} \cdot \delta v dV \tag{13}$$

where $\ddot{u}$ is the acceleration field. When implicit integration is used, the equilibrium equations are written at the end of a time step (at time $t + \Delta t$), and $\ddot{u}$ is calculated from the time integration operator. The interpolator approximates the displacement at a point as

$$u = N^N u^N \tag{14}$$

where N^N is interpolation vector, and it is not displacement dependent, u^N is nodal displacement vector, so that

$$\ddot{u} = N^N \ddot{u}^N \tag{15}$$

With this interpolation assumption, the inertia force-related term is

$$-\left(\int_V \rho N^N \cdot N^M dV\right)\ddot{u}^M \tag{16}$$

that is, the consistent mass matrix times the accelerations of the nodal variables. The finite element approximation to equilibrium is

$$M^{NM}\ddot{u}^M + I^N - P^N = 0 \tag{17}$$

where $M^{NM} = \int_V \rho N^N \cdot N^M dV$ is the consistent mass matrix, I^N is the internal force vector and the effect of friction force is contained in this term, and P^N is the external force vector.

The implicit integration operator replaces the actual equilibrium equation Eq. (17) with a balance of inertia forces at the end of the time step and a weighted average of the static forces at the beginning and end of the time step:

$$M^{NM}\ddot{u}^M|_{t+\Delta t} + (1+\alpha)\left(I^N|_{t+\Delta t} - P^N|_{t+\Delta t}\right) - \alpha\left(I^N|_t - P^N|_t\right) + L^N|_{t+\Delta t} = 0 \tag{18}$$

where $L^N|_{t+\Delta t}$ is the sum of all Lagrange multiplier forces associated with degree of freedom N. In the Newmark scheme the formulae for displacement and velocity integration are:

$$u|_{t+\Delta t} = u|_t + \Delta t\dot{u}|_t + \Delta t^2\left((1/2-\beta)\ddot{u}|_t + \beta\ddot{u}|_{t+\Delta t}\right) \tag{19}$$

$$\dot{u}|_{t+\Delta t} = \dot{u}|_t + \Delta t\left((1-\gamma)\ddot{u}|_t + \gamma\ddot{u}|_{t+\Delta t}\right) \tag{20}$$

with

$\beta = \left(1-\alpha^2\right)/4$, $\gamma = 1/2-\alpha$ and $-1/3 \le \alpha \le 0$

In the implicit dynamic analysis procedure, two factors should be considered when selecting the maximum allowable time step size: the rate of variation of the applied loading and the typical period of vibration of the structure. In general, a maximum increment versus period ratio $\Delta t/T < 1/10$ is a good rule of thumb for obtaining reliable results. As known, the frequencies of rail corrugation always fall in the range 60-500Hz [1-4]. Therefore, the maximum increment of the implicit time integration is set to 0.00005s (20000Hz).

In the present work, two finite element analysis methods are applied to study the dynamic response of the wheelset-track system by using Abaqus/Standard. One is the dynamic transient analysis. Its calculation process is described above. The other is the complex eigenvalue analysis, Ouyang [28] and Chen et al. [17] made a detailed description of the calculation process of this method in their publications.

To perform the dynamic transient analysis of the wheelset track system, two main steps are required as follows:

Step 1: nonlinear static analysis of the wheelset track system for applying the suspension force on the wheelset.

Step 2: nonlinear implicit dynamic analysis of the wheelset track system for calculating the transient dynamic response.

In the dynamic transient analysis, the element type is C3D8R (8-node linear brick, reduced integration), the contact formulation is kinematic method, the sliding formulation is finite sliding and the friction formulation is the penalty method.

To perform the complex eigenvalue analysis, four main steps are required as follows:

Step 1: The same as the transient analysis.

Step 2: nonlinear static analysis to impose the sliding speed on the wheelset.

Step 3: normal mode analysis to extract natural frequency without the friction coupling.

Step 4: complex eigenvalue analysis that incorporates the effect of friction coupling.

In the complex eigenvalue analysis, the element type is C3D8I (8-node linear brick, incompatible modes). The contact formulation is finite sliding with the penalty method. The friction formulation is the penalty method.

3. Results and discussion

3.1 Relations between the self-excited vibration of the wheelset-track system and the corrugation wear of the rail

This section presents the results of the transient dynamic simulations when the wheelset negotiates a tight curved track. In the transient dynamic analysis, the initial translational and rotational velocities of the wheelset are 70km/h and 46.296rad/s (corresponding to the nominal wheel diameter of 840mm). When the wheelset travels on the rail, only the suspension forces are applied on the wheelset without any other external excitations. This is different from the conventional vehicle dynamics analysis. Under these conditions, self-excited vibration of the wheelset and the rail may arise. Under the dry and clean conditions, the friction coefficient between the wheel and rail always larger than 0.3[29]. Therefore, when the effect of saturated creep force is considered on the wheel rail system, the friction coefficient is set to 0.45. Such results are compared with the results when there is no friction (the friction coefficient is taken to be zero), in order to reveal the influence of friction between wheel and rail.

Fig. 4 shows the vibration accelerations of the rail surface in the normal direction. From Fig. 4a, it is found that the oscillation amplitude of vibration accelerations on the low rail surface increase significantly when friction coefficient μ becomes 0.45. Fig. 4b shows that the vibration accelerations on the high rail increase slightly when friction

coefficient becomes μ =0.45. A comparison between the vibration accelerations of the low and the high rails is shown in Fig. 4c. It can be found that the oscillation amplitude of vibration accelerations on the low rail surface is obviously greater than that on the high rail surface. This simulation result demonstrates that the self-excited vibration probably takes place on the low rail. Fig. 5 shows the variations of the normal contact forces in time domain. The normal contact force is the sum of normal contact pressure in the contact zone in the direction perpendicular to the contact surface. When the wheelset negotiates a curved track, the contact point between the outer wheel of the wheelset and high rail is at the flange root of the wheel, and the contact point between the inner wheel and low rail is at the center of the wheel tread (Fig. 3c). These contact differences lead to the average normal load of around 110 kN on low rail and 80 kN on high rail. The normal contact forces between the wheels and rails when the friction coefficient μ = 0 are shown in Fig. 5a. It can be found that the oscillation amplitude of normal contact forces is very small. Fig. 5b shows the normal contact forces between the wheels and rails when friction coefficient μ increases to 0.45. Comparing Fig. 5b with Fig. 5a, it can be found that with the increase of the friction coefficient μ, the oscillation amplitude of normal contact force on the low rail significantly increases. The oscillation amplitude of normal contact force on the high rail increase slightly when μ becomes 0.45. It can be observed that the variations of the normal contact forces are consistent with the changes of the vibration accelerations. This phenomenon demonstrates that the friction induced self-excited vibration of the wheelset-track system can lead to fluctuation of the normal contact force.

To further analyze the correlation between the self-excited vibrations and the fluctuation of the normal contact force, the power spectral density (PSD) analyses is made. Fig. 6 shows the PSD results of unstable vibration accelerations on the rail surface in the normal direction. The unstable vibration on the low rail is characterized by one main frequency of 407.71Hz as shown in Fig. 6a. The unstable vibration on the high rail is characterized by one main frequency of 415.03Hz (Fig. 6b), which is slightly different from the main vibration frequency of the low rail. Fig. 7 shows the PSD of the normal contact force. The main vibration frequencies of the normal contact force on low and high rails are 407.71Hz (Fig. 7a) and 415.03Hz (Fig. 7b), respectively. It can be found that the main unstable vibration frequencies of the normal contact forces are the same as the frequencies of unstable vibration accelerations. This phenomenon also

demonstrates that the oscillation of normal contact force is induced by self-excited vibration of the wheel and rail.

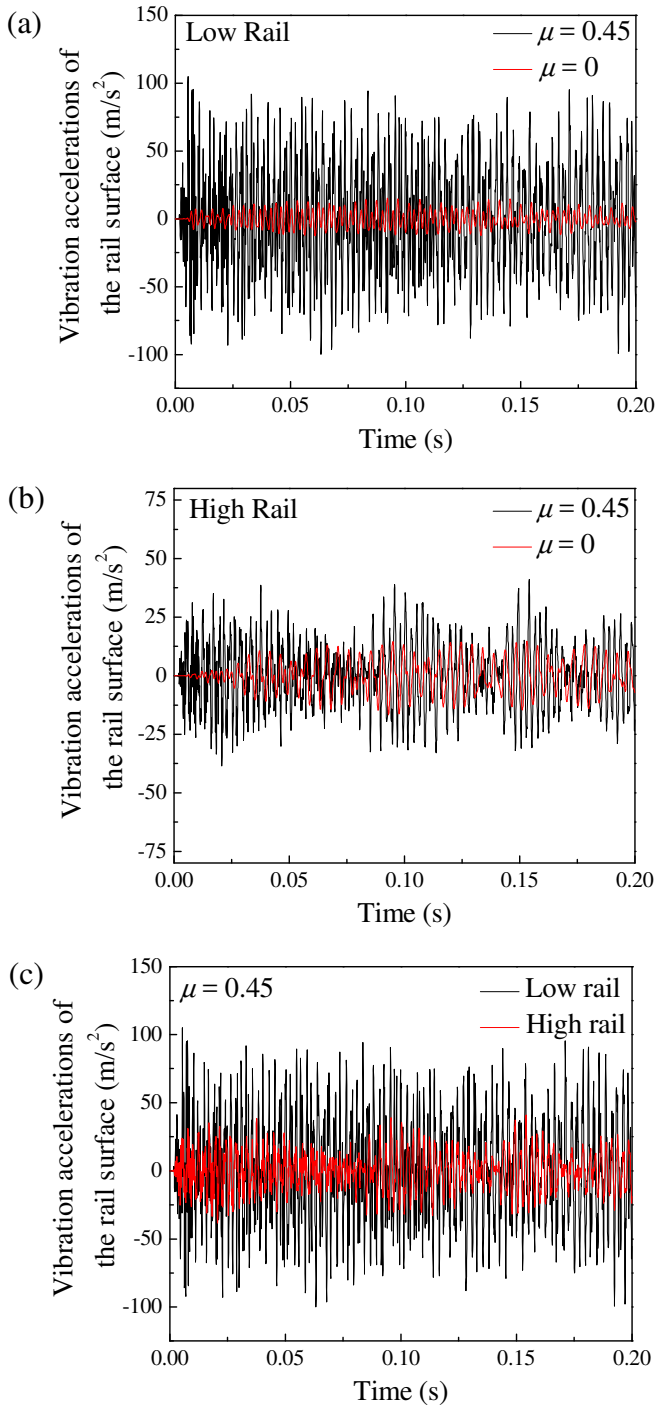

Fig. 4. Vibration acceleration of the rail surface: (a) low rail surface with different friction coefficient; (b) high rail surface with different friction coefficient; (c) a comparison between the high rail and low rail surfaces.

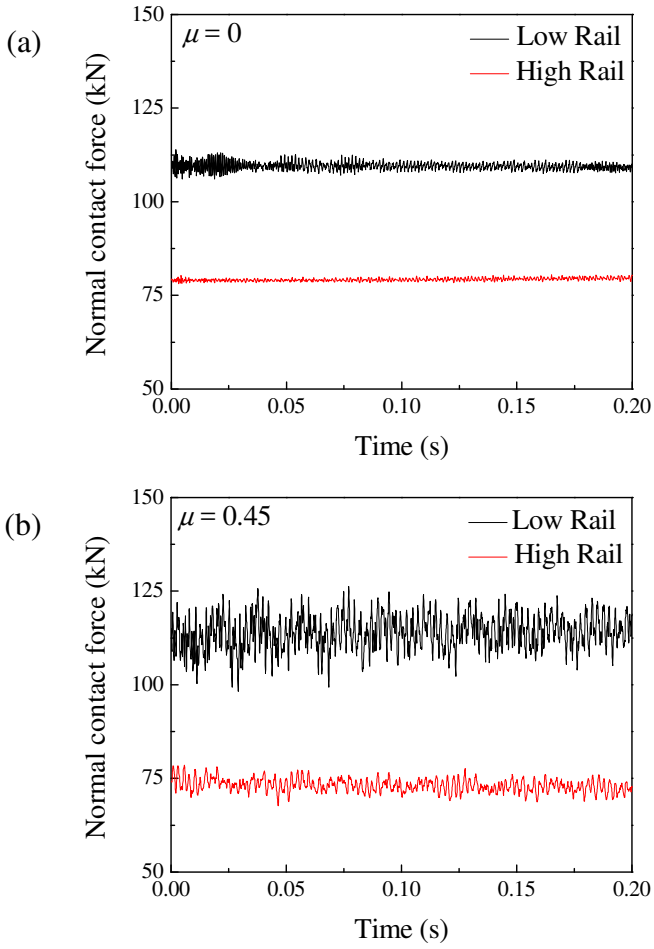

Fig. 5. Normal contact force between the wheel and rail: (a) friction coefficient μ = 0; (b) μ = 0.45.

In the railway research community, it is generally accepted that fluctuating friction work results in undulant wear of rails [7, 30]. Therefore, the friction work rate approach is useful in studying corrugation formation in relation to the self-excited vibration. Brockley [14] developed a wear equation of rails. A modified version of this equation expressed in terms of wear volume per unit of time is

$$w = K(H - C)$$

where w is wear volume per unit of time, K is the wear constant, H is the friction work rate ($H = FV$), F is the creep force, V is the relative velocity and C is the durability friction work rate.

When the lateral creep force F is saturated, $F = \mu N$, where μ is the friction coefficient between the wheel and rail and N is the normal contact force. Lateral velocity of the wheelset $V = \psi \times v$, where ψ is the angle of attack of the wheelset and v is the forward speed of the wheelset. In the transient dynamics simulation process ψ,

v and μ are set to constant. From Figs. 4 and 5, it is found that when self-excited vibration occurs, normal contact forces between the wheels and rails fluctuate at the same frequencies. Therefore it can be concluded that friction work rate H fluctuates when self-excited vibration occurs. According to Brockley [14], such a fluctuating friction work rate can result in rail corrugation.

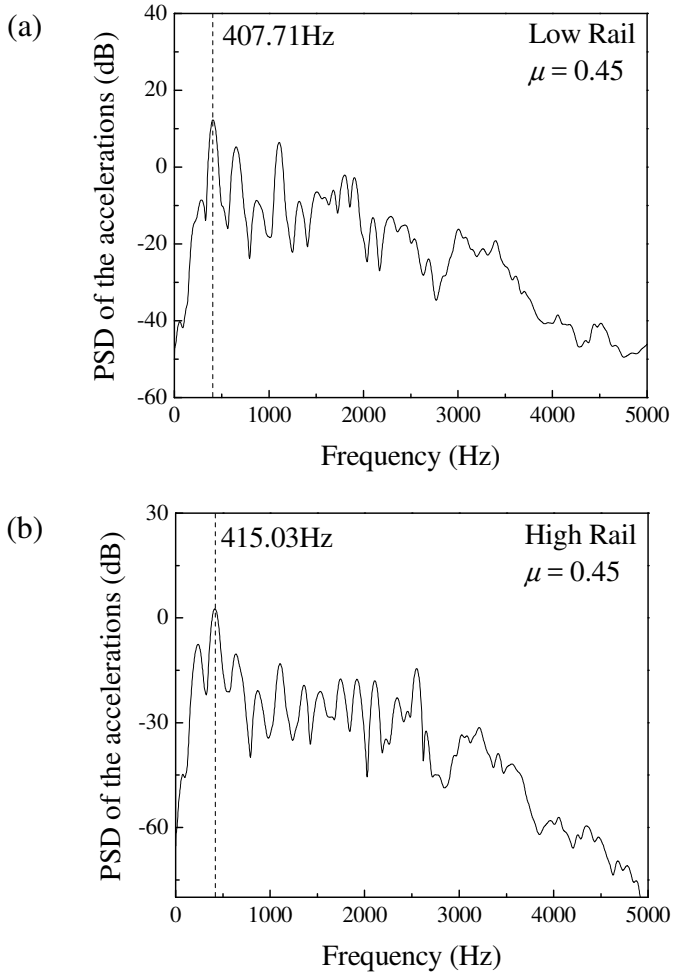

Fig. 6. PSD of the vibration acceleration of the rail surface shown in Fig. 4: (a) low rail; (b) high rail.

In the present work, the vibration frequency of the normal contact force on the low rail is 407.71Hz, and on the high rail is 415.03Hz. The wave length of the corresponding rail corrugation are l_{Low}= 47.7mm on the low rail and l_{High} = 46.8mm on the high rail (forward speed of the vehicle v = 70km/h), which is a short wave length corrugation. Furthermore, from Fig. 5b, it can be found that the oscillation amplitude of the normal contact force on the low rail is significantly greater than that on the high rail.

It may be inferred that a short wave length rail corrugation on tight curves most probably takes place on the low rail.

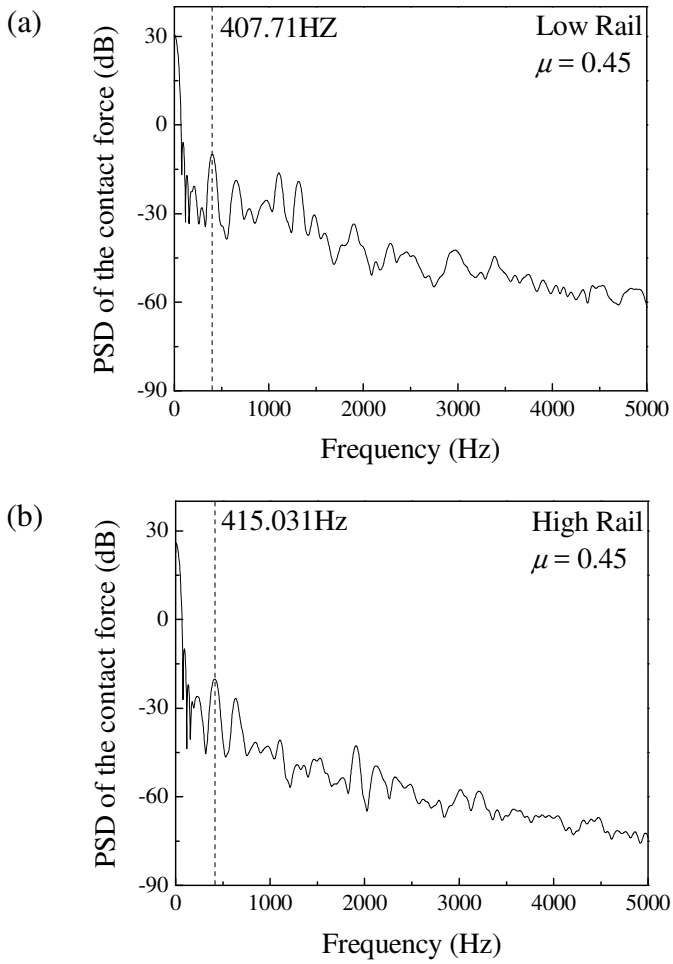

Fig. 7. PSD of the normal contact force shown in Fig. 5b: (a) low rail; (b) high rail.

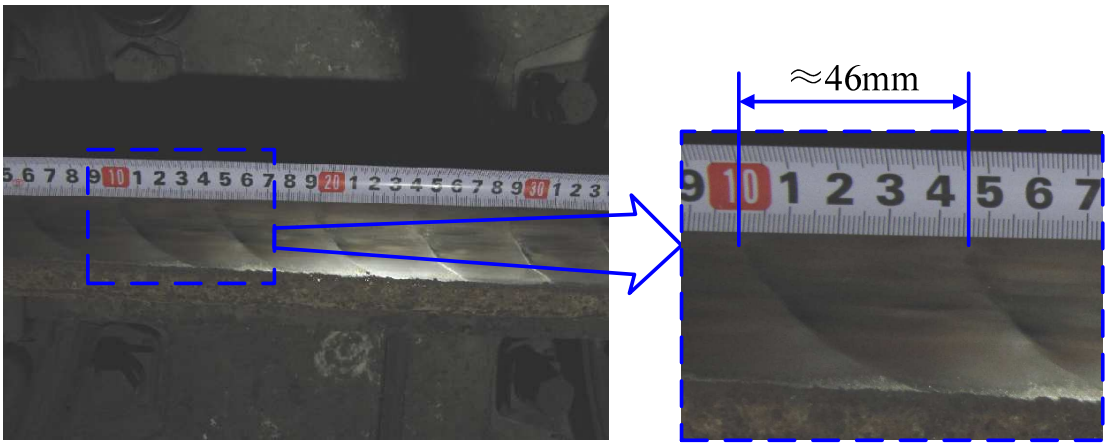

Fig. 8. Short pitch corrugation on the low rail of the curved track in Beijing metro: wave length of the rail corrugation $l_{\text{Low}} \approx 0.046$m.

In railway lines, severe corrugations usually occur on curved tracks, especially on the low rail [31]. Fig. 8 shows short pitch corrugations on the low rail of the curved track with a radius of 300m in Beijing metro. The average running speed of the measured section is about 70 km/h. It can be found that the wave length of the corrugation is about 46mm. The simulation result is very close to the measured result.

3.2 Mode shapes of unstable vibrations on a tight curve

Finite element complex eigenvalue analysis is thought to be an effective method available to predict unstable propensity of friction sliding systems [28]. In the present work, finite element complex eigenvalue analysis is also applied to study stability of the wheelset-track system due to the saturated creep force coupling. For the wheelset-track system shown in Fig. 3, the complex eigenvalue analysis shows that there is one unstable mode when friction coefficient μ = 0.45. Fig. 9 shows the unstable mode shape. It is seen that self-excited vibration probably takes place on the low rail and the wheel. This is consistent with the transient dynamic analysis results. The complex eigenvalue analysis predicts that the unstable frequency of the wheelset-track system is 463.69Hz as shown in Fig. 10. The wave length of rail corrugation on the low rail l_{Low}= 41.9mm when forward speed of the vehicle v = 70km/h. Comparing the dynamic analysis result with the complex eigenvalue analysis result, it can be found that the difference between the unstable vibration frequencies (407.71Hz and 463.69Hz) is approximately 10%. This is because the complex eigenvalue analysis and the transient dynamic analysis use different methods to solve the motion equation of the friction system. The complex eigenvalue analysis calculates the general solution of the equations of motion by using the subspace projection method. This is a frequency domain approach. One the other hand, the transient dynamic analysis uses the implicit time integration to calculate the dynamic response of the friction system in the time domain. The two approaches are known to produce different results that should not be far away from each other, which is confirmed the above results of frequencies.

Based on the transient dynamic simulation results, the complex eigenvalue analysis results and the measured data on Beijing metro, it can be concluded that self-excited vibration induced by the saturated creep force is probably responsible for rail corrugation. And the self-excited vibration induced short wave length rail corrugation most probably takes place on the low rail when the wheelset negotiates a tight curved track.

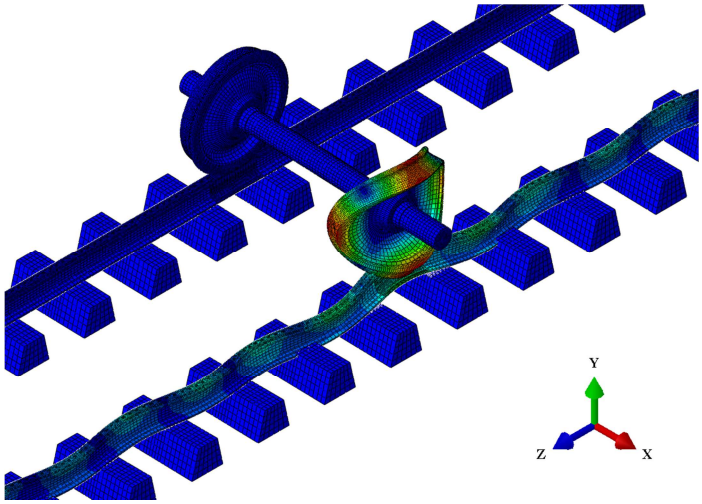

Fig. 9. Mode shape of unstable vibration on a tight curve track, μ = 0.45, unstable vibration frequency f_R = 463.69Hz, damping ratio ζ = -0.02163.

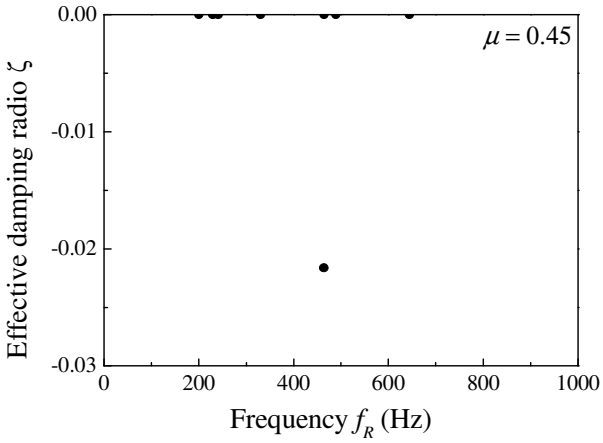

Fig. 10. Unstable frequency of vehicle travelling on a tight curve track, μ = 0.45, f_R = 463.69Hz, ζ = -0.02163.

3.3 Transient dynamic analysis of the self-excited vibration of the wheelset-track system on a straight track

Trains undergo very large longitudinal traction forces or brake forces when they are accelerated or are braked. If these longitudinal traction forces or brake forces become saturated, that is, equal to the normal forces multiplied by the dynamic coefficient of friction, these saturated creep forces also can induce self-excited vibration of the wheelset-track system. In the transient dynamic simulation process, the initial translational and rotational velocities of the wheelset are 120km/h and 79.3651rad/s (the nominal diameter of the wheelset is 840mm). A translational acceleration of 0.55m/s^2 is applied on the wheelset to simulate the speed up process of the vehicle. There is no

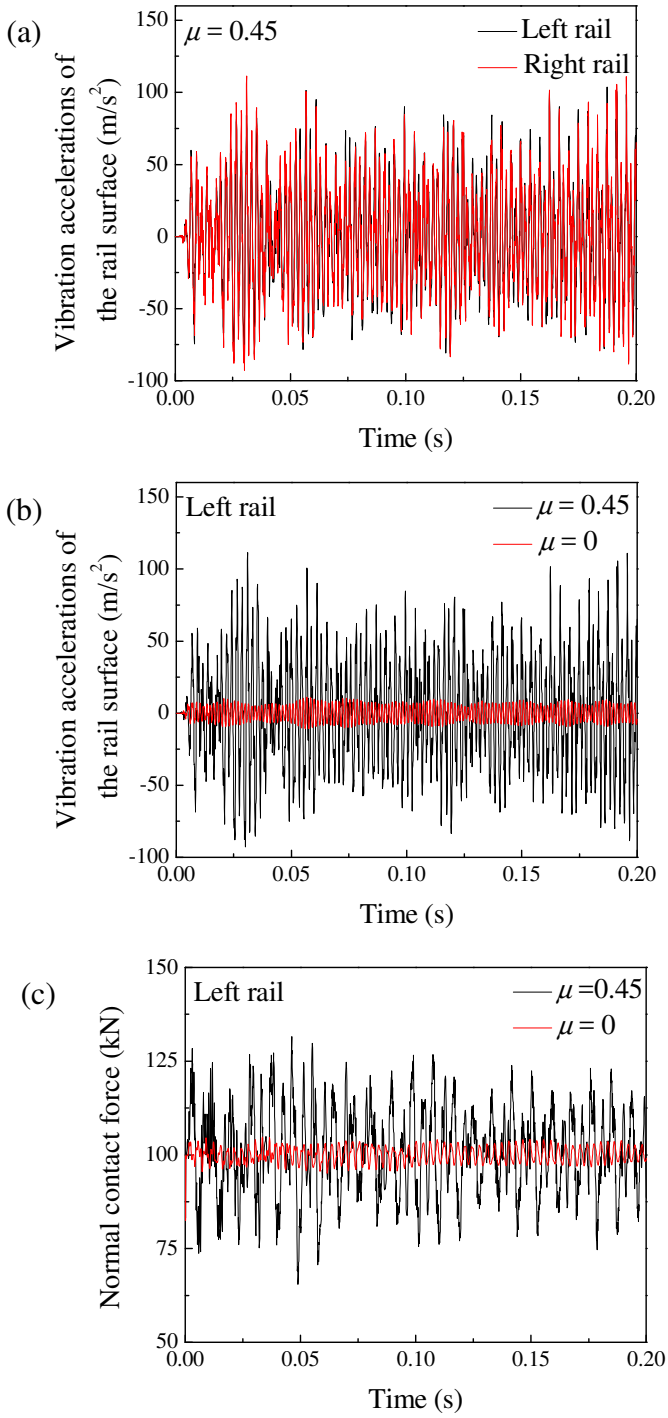

Fig. 11. Transient dynamic simulation results of the wheelset-track system on a straight track: (a) vibration accelerations on the left and right rail surface; (b) variation of the vibration acceleration on the left rail surface; (c) variation of the normal contact force.

external excitation applied on the wheelset and the track. Fig. 11 shows the transient dynamic simulation results of the wheelset-track system on a straight track. When the wheelset travels on a straight track, the contact conditions between the wheelset and the rails are exactly symmetrical. Therefore, the vibration response of the left and the right

rails are almost the same as shown in Fig. 11a. Fig. 11b shows the vibration accelerations of the left rail when friction coefficient μ = 0 and 0.45. It is seen that the self-excited vibration of the rail can be induced by the saturated creep force. Fig. 11c shows the variation of the normal contact force between the wheelset and the left rail. It can be found that the oscillation amplitude of the normal contact force on the left rail increase significantly when there is friction at the wheelset-rail interface. The main unstable vibration frequency of rail surface and the normal contact force is 471.19Hz as shown in Fig. 12a and b. The wave length of corrugation on tangent tracks is evaluated to be l = 70.7mm at the speed of 120km/h.

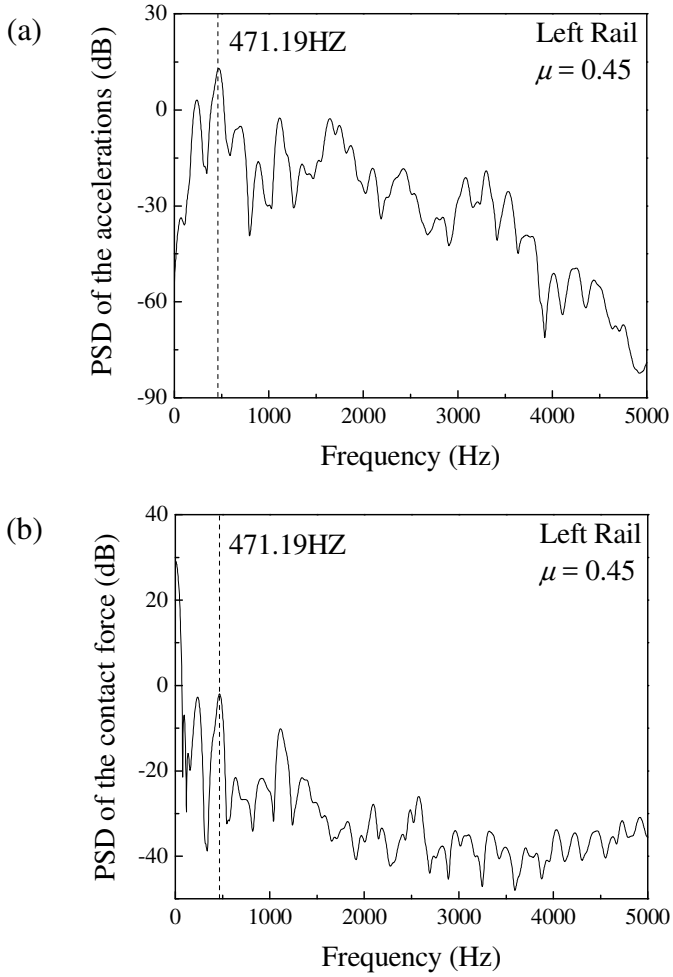

Fig. 12. PSD of the transient dynamic simulation results: (a) PSD of the vibration acceleration shown in Fig. 11b; (b) PSD of the normal contact force shown in Fig. 11c.

3.4 Mode shapes of unstable vibrations on a straight track

The complex eigenvalue analysis shows that there are two unstable frequencies (264.74Hz and 448.49Hz) when the wheelset travels on a straight track. The mode

shapes of unstable vibrations are shown in Fig. 13. From Fig. 13a, it is seen that self-excited vibration most probably takes place on the wheel. From Fig. 13b, it is seen that self-excited vibration also probably takes place on the rail. It is found that the mode shown in Fig. 13b has a damping ratio of ζ = -0.0052. This damping ratio is the larger one (in absolute value) in these two damping ratios of unstable modes and suggests that the mode shown in Fig. 13b occurs more easily. The vibration frequency of this unstable mode is 448.49Hz (Fig. 14). It is fairly close to the frequency from the transient dynamic analysis (471.19Hz). The wave length of corrugation on tangent tracks is evaluated to be l = 125.9mm for the unstable frequency f_R = 264.74Hz at a speed of 120km/h and l = 74.3mm for the unstable frequency f_R = 448.49Hz at a speed of 120km/h.

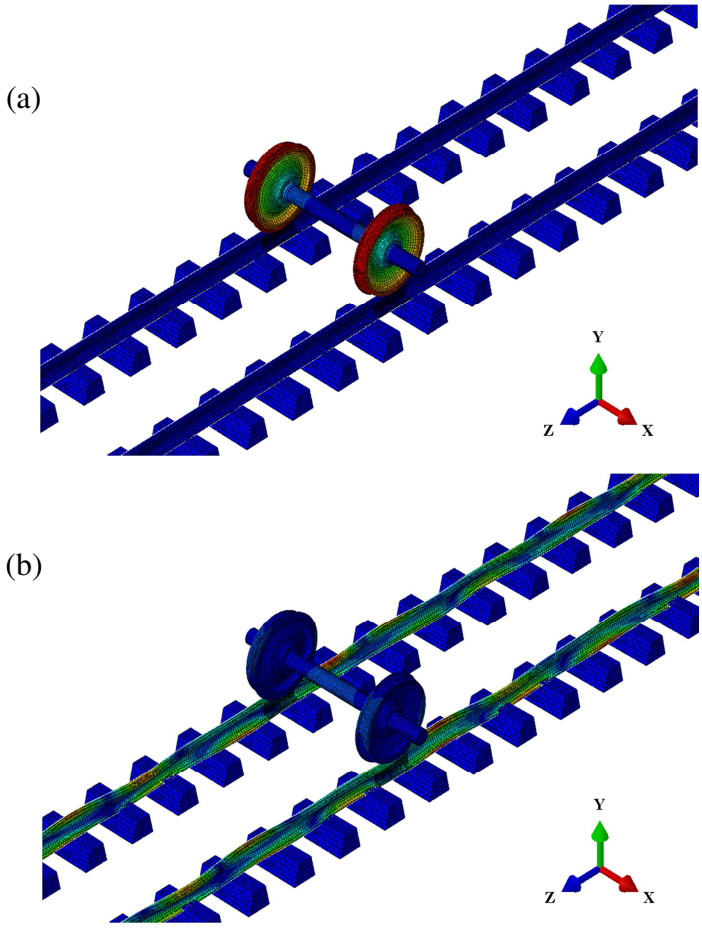

Fig. 13. Mode shape of unstable vibration on a straight track, μ = 0.45: (a) f_R = 264.74Hz, ζ = -0.0035; (b) f_R = 448.49Hz, ζ = -0.0052.

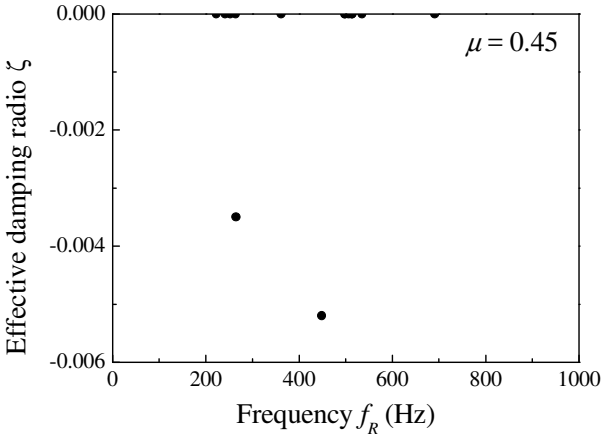

Fig. 14. Unstable frequencies of vehicle travelling on straight track, μ = 0.45, f_R = 264.74Hz and 448.49Hz; ζ = -0.0035 and -0.0052.

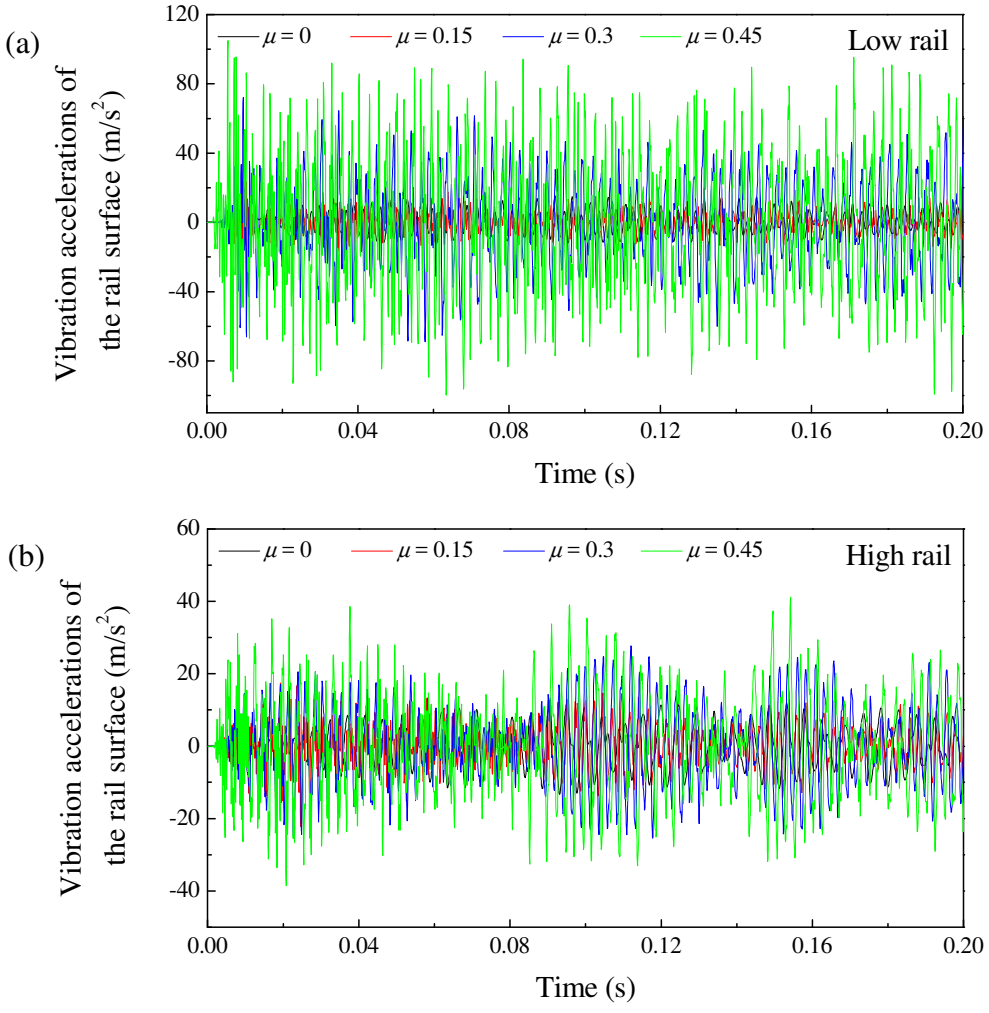

Fig. 15 Evolution of the vibration accelerations on the rail surfaces at different friction coefficient: (a) Low rail; (b) High rail.

3.5 Parameter sensitivity analysis

In this section, the dynamic transient simulations are performed for the parameter sensitivity analysis of the wheelset track system. Because severe corrugations usually occur on curved tracks, the parameter sensitivity analysis is focused on the curved track model.

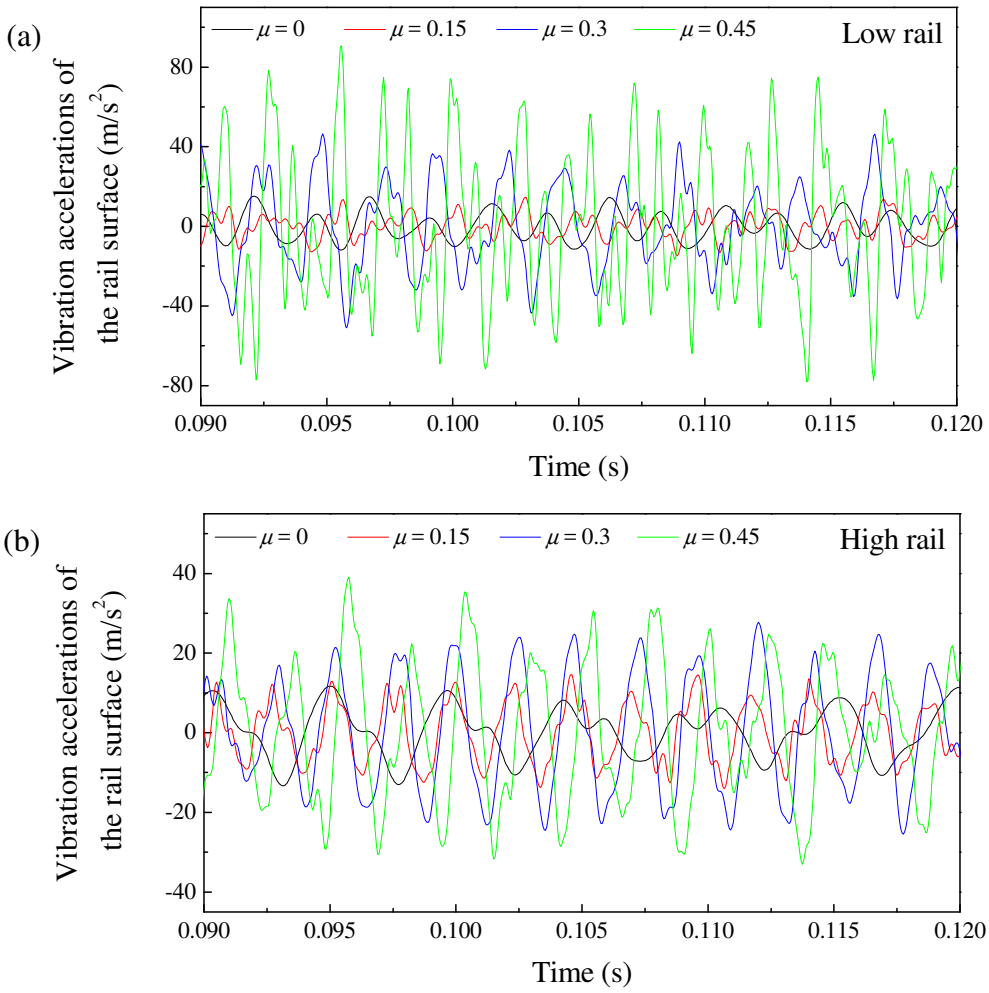

Fig. 16 Variation details of the vibration accelerations on the rail surfaces with different friction coefficient: (a) Low rail; (b) High rail.

3.5.1 Effect of friction coefficient on self-excited vibration of the wheelset-track system on a tight curve

The friction coefficient has a significant effect on self-excited vibration of the wheelset-track system. Fig. 15 shows the evolution of the vibration accelerations on the low (Fig. 15a) and high (Fig. 15b) rail surfaces with different friction coefficient μ. It is seen that with the increase of the friction coefficient, the oscillation amplitude of the

vibration accelerations increase significantly. Fig. 16 shows the variation details of the vibration accelerations on the low (Fig. 16a) and high (Fig. 16b) rail surfaces. When the friction coefficient increases from 0 to 0.15, the oscillation amplitude of the vibration accelerations increase slightly. When the friction coefficient increases from 0.15 to 0.3 or from 0.3 to 0.45, the oscillation amplitude of the vibration accelerations increase significantly. This phenomenon indicates that the friction induced self-excited vibration of the wheelset-track system is inconspicuous when the friction coefficient at a low level. And when the friction coefficient reaches a larger value, the self-excited vibrations of the wheelset-track system will become obvious. Keeping the friction coefficient at a low level may help to eliminate rail corrugation. Fig. 17 shows the variation of the self-excited vibration frequencies with different friction coefficient. It can be observed that with increasing friction coefficient, the frequency corresponding to the self-excited vibration decreases slightly. This suggests that the friction coefficient has a little influence on the frequency of self-excited vibration.

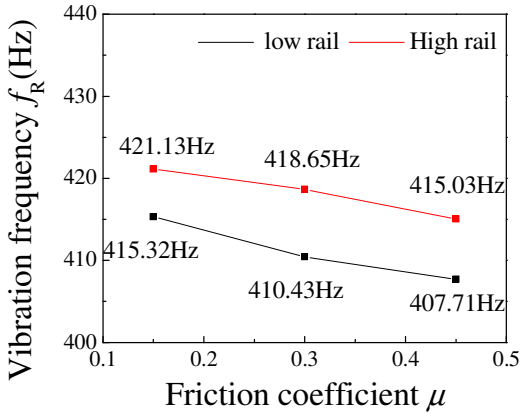

Fig. 17 Vibration frequency variation with friction coefficient.

3.5.2 Influence of damping of the rail fastener

In the present work, the dynamic transient simulations are performed for different levels of damping of the rail fastener. Because severe corrugations usually occur on curved tracks, the parameter sensitivity analysis is focused on the curved track model. The simulation results show that the rail fastener damping has a significant effect on self-excited vibration when the wheelset negotiates a curved track. Fig. 18 shows the variation of the normal contact force at several different levels of rail fastener damping on a curved track. It can be found that with the increase of the rail fastener damping (from half of its normal value increase to its normal value) the oscillation amplitude of

the normal contact forces on low (Fig. 18a) and high (Fig. 18b) rails significantly decreases. This result suggests that rail fastener damping can reduce the oscillation amplitude of normal contact force between the wheel and rail. Increasing the damping of the rail fastener may help to suppress rail corrugation. However, the oscillation amplitude of normal contact force decrease slightly when the rail fastener damping increase to two times its normal value. This phenomenon demonstrates that the rail fastener damping cannot eliminate all self-excited vibrations of the wheelset-track system.

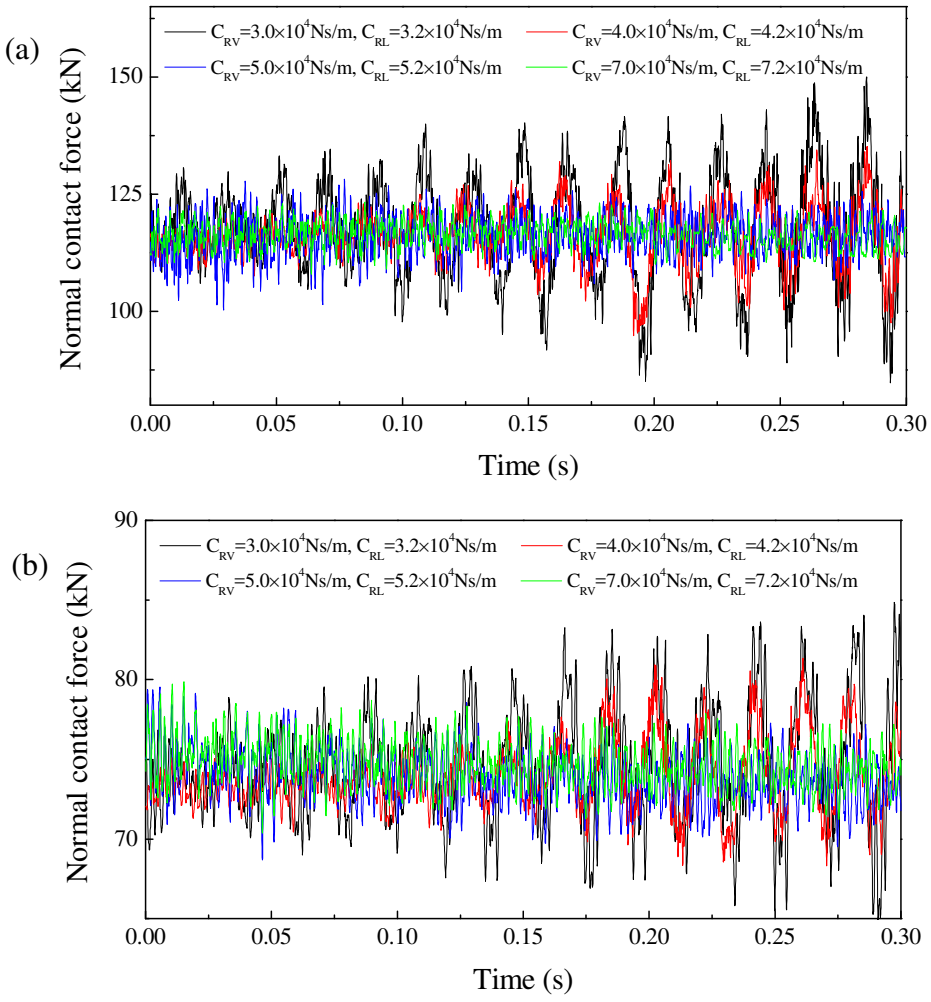

Fig. 18. Variation of the normal contact force with rail fastener damping on curved track, (a) low rail; (b) high rail.

3.5.3 Influence of the stiffness of the rail fastener

Fig. 19 shows the variation of the normal contact force at several different levels of rail fasteners stiffness on a curved track. It can be found that the stiffness of the rail

fastener has a small influence on the oscillation amplitude of the normal contact force. Fig. 19a shows the variation of the normal contact force on the low rail. It is seen that with the increase of the rail fastener stiffness, the oscillation amplitude of normal contact force decreases slightly. Fig. 19b shows the variation of the normal contact force on the high rail. It also can be observed that the rail fastener stiffness has a small influence on the normal contact force on the high rail.

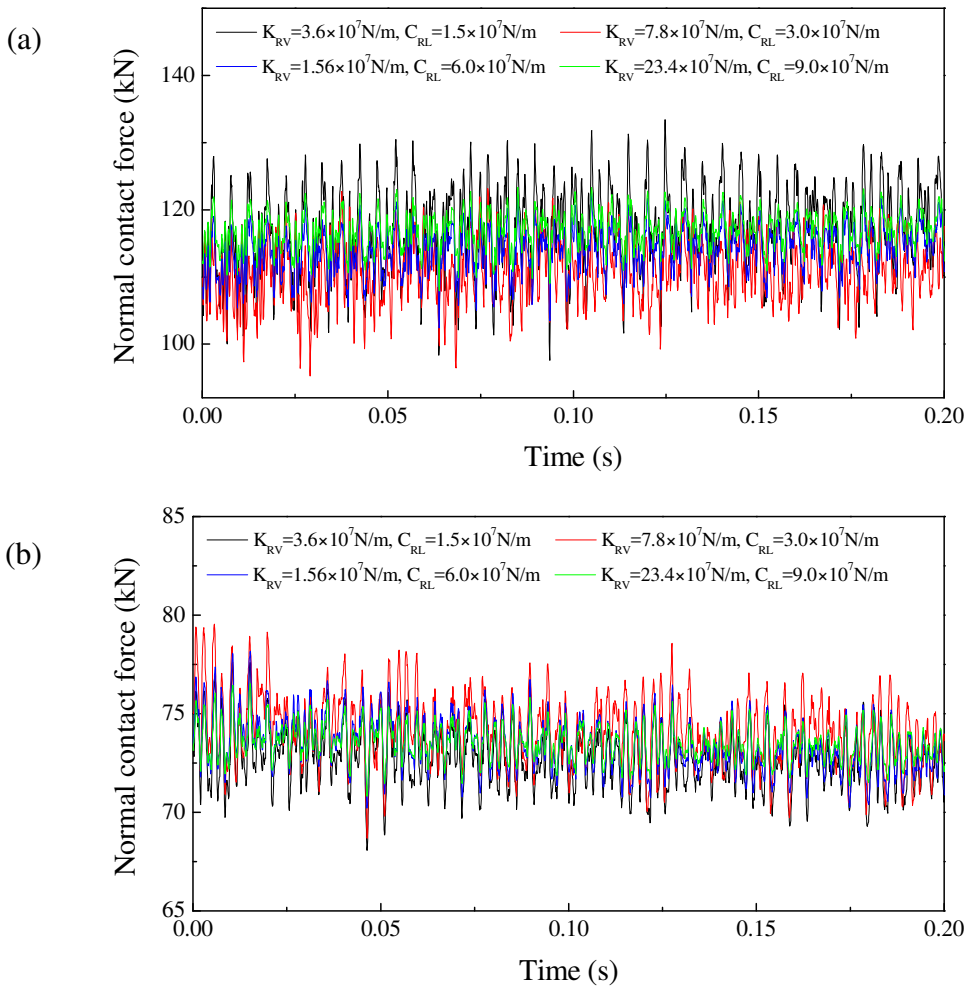

Fig. 19. Variation of the normal contact force with rail fastener stiffness on curved track, (a) low rail; (b) high rail.

4. Conclusions

This paper presents a numerical study of wear-type rail corrugation based on saturated creep force-induced self-excited vibration of a wheelset-track system. Two finite element models consisting of a wheelset, rails, sleepers and support springs and dampers are established and analyzed using the transient dynamic and complex

eigenvalue methods. In the models, it is assumed that creep forces between wheels and rails are saturated when the wheelset negotiates a sharp curve, or travels on a straight track during acceleration or braking. The following conclusions can be drawn.

(1) The saturated creep forces between the wheel and rail can induce self-excited vibration of the wheelset-track system. When the self-excited vibration occurs, normal contact force between the wheel and rail fluctuates at the same frequency. Such a fluctuating normal contact force can result in rail corrugation.

(2) The dynamic transient and complex eigenvalue analyses results show that the self-excited vibration induced short wave length rail corrugation on tight curves most probably takes place on the low rail.

(3) The parameter sensitivity analysis shows that the friction coefficient and rail fastener damping have significant effect on the self-excited vibration induced rail corrugation. The stiffness of rail fastener has a small influence on the self-excited vibration induced rail corrugation.

Acknowledgements

This research received the financial supports from National Natural Science Foundation of China (No. 51275429), the innovation team development plan of the ministry of education (IRT1178) and the Fundamental Research funds for the Central University (SWJTU12ZT01). The third author wishes to acknowledge the support of Changjiang Scholarship.

References

[1] Sato Y., Matsumoto A., Knothe K., Review on rail corrugation studies, *Wear* 253 (2002), pp. 130-139.

[2] Grassie S. L., Kalousek J., Rail corrugation: characteristics, causes and treatments, *Journal of Rail Rapid Transit* 207 (1993), pp. 57-68.

[3] Grassie S. L., Rail corrugation: advances in measurement, understanding, and treatment, *Wear* 258 (2005), pp. 1224-1234.

[4] Oostermeijer K. H., Review on short pitch rail corrugation studies, *Wear* 265 (2008), pp. 1231-1237.

[5] Knothe K., Ripke B., The effects of parameters of wheelset, tract and running conditions on the growth rate of rail corrugation, in: *Dynamics of Vehicles on Roads and on Tracks, Proc. 11th IAVSD Symposium*, Kingston, Ontario, Canada 18 (1989), pp. 345-356.

[6] Hempelmann K., Knothe K., An extended linear model for the prediction of short pitch corrugation, *Wear* 191 (1996), pp. 161-169.

[7] Muller S., A linear wheel-rail model to investigate stability and corrugation on straight track, *Wear* 249 (2001), pp. 117-1127.

[8] Nielsen J. B., Evolution of rail corrugation predicted with a non-linear model, *Journal of Sound and Vibration* 227 (5) (1999), pp. 915-933.

[9] Jin X. S., Wen Z. F., Wang K. Y., Effect of track irregularities on initiation and evolution of rail corrugation, *Journal of Sound and Vibration* 285 (1–2) (2005), pp. 121-148.

[10] Xie G., Iwnicki S.D., Calculation of wear on a corrugated rail using a three-dimensional contact model, *Wear* 265 (2008), pp. 1238–1248.

[11] Xie G., Iwnicki S.D., Simulation of wear on a rough rail using a time-domain wheel-track interaction model, Wear 265 (2008), pp. 1572-1583.

[12] Clark R. A., Slip-stick vibrations may hold the key to corrugation puzzle, *Railway Gazette International* 7 (1984), pp. 531-533.

[13] Clark R. A., Scott G. A., Poole W., Short wave corrugation-an explanation based on stick-slip vibrations, in: *Proceedings of the Applied Mechanics Rail Transportation Symposium 96 ASME*, 1988, pp.141-148.

[14] Brockley C. A., An investigation of rail corrugation using friction-induced vibration theory, *Wear* 128 (1988), pp. 99-106.

[15] Ishida M., Moto T., Takikawa M., The effect of lateral creepage force on rail corrugation on low rail at sharp curves, *Wear* 253 (2002), pp. 172-177.

[16] Wu T. X., Thompson D. J., An investigation into rail corrugation due to micro-slip under multiple wheel/rail interactions, *Wear* 258 (2005), pp. 1115-1125.

[17] Chen G. X., Zhou Z. R., Ouyang H., Jin X. S., Zhu M. H., and Liu Q. Y., A finite element study on rail corrugation based on saturated creep force-induced self-excited vibration of a wheelset–track System, *Journal of Sound and Vibration* 329 (2010), pp. 4643–4655.

[18] Kurzeck B., Hecht M., Dynamic simulation of friction induced vibrations in a light railway bogie while curving compared with measurement results, *Vehicle System Dynamics* 48(Supplement 1) (2010), pp. 121-138.

[19] Kurzeck B., Combined friction induced oscillations of wheelset and track during the curving of metros and their influence on corrugation, *Wear* 271(1-2) (2011), pp. 299 -310.

[20] Eadie D. Santoro T., M., Oldknow K., Oka Y., Field studies of the effect of friction modifiers on short pitch corrugation generation in curves, *Wear* 265 (2008), pp. 1212-1221.

[21] Tomeoka M., Kabe N., Tanimoto M., Miyauchi E., Nakata M., Friction control between wheel and rail by means of on-board lubrication, *Wear* 253 (2002), pp. 124-129.

[22] Garg V. K., Dukkipati R. V., Dynamics of Railway Vehicle Systems, *Academic press*, New York, USA, 1984.

[23] Blader F. B., Elkins J. A., Wilson N. G., Klauser P. E., Development and validation of a general railroad vehicle dynamics simulation (NUCARS), in: *Proceedings of the ASME/IEEE Joint Railroad Conference*, Philadelphia, PA, April (1989).

[24] Zhong Z. H., Contact Problems with Friction, in: *Proceedings of Numiform* 89, Balkema, Rotterdam (1989), pp. 599–606.

[25] Oden J. T., Pires E. B., Nonlocal and Nonlinear Friction Laws and Variational Principles for Contact Problems in Elasticity, *Journal of Applied Mechanics* 50 (1983), pp. 67–73.

[26] Hilber H. M., Hughes T. J. R., Taylor R. L., Improved Numerical Dissipation for Time Integration Algorithms in Structural Dynamics, *Earthquake Engineering and Structural Dynamics* 5 (1977), pp. 283–292.

[27] Czekanski A., El-Abbasi N., Meguid S. A., Optimal Time Integration Parameters for Elastodynamic Contact Problems, *Communications in Numerical Methods in Engineering* 17 (2001), pp. 379–384.

[28] Ouyang H., Nack W., Yuan Y., Chen F., Numerical analysis of automotive disc brake squeal: a review, *International Journal of Vehicle Noise Vibration* 1(3/4) (2005), pp. 207-231.

[29] Jin X. S., Liu Q. Y., Tribology of wheel and rail, China Railway Publishing House, Beijing, China 2004.

[30] Igeland A., Ilias H., Rail head corrugation growth predictions based on nonlinear high frequency vehicle/track interaction, *Wear* 213 (1997), pp. 90-97.

[31]Jin X. S., Wen Z. F., Effect of discrete track support by sleepers on rail corrugation at a curved track, Journal of Sound and Vibration 315 (2008), pp. 279-300.